**EARTH'S CRYOSPHERE**
SCIENTIFIC JOURNAL

*Kriosfera Zemli*, 2019, vol. XXIII, No. 4, pp. 22–30 **http://www.izdatgeo.ru**

*GEOCRYOLOGICAL MONITORING AND FORECAST*

DOI: 10.21782/EC2541-9994-2019-4(22-30)

# IMPACTS OF CLIMATE CHANGE ON LONG-TERM DYNAMICS OF SEASONAL FREEZING IN MOSCOW REGION: RETROSPECTIVE ANALYSIS AND UNCERTAINTIES IN FORECASTING FOR THE SECOND HALF OF THE 21st CENTURY

**S.P. Pozdnyakov, S.O. Grinevskyi, E.A. Dediulina**

*Lomonosov Moscow State University, Faculty of Geology, Department of Hydrogeology, 1, Leninskie Gory, Moscow, 119991, Russia; sppozd@mail.ru*

A quantitative analysis of the forecast dynamics of seasonal freezing depth in the 21st century has been carried out using climate projections obtained by 5 models of the Atmosphere-Ocean General Circulation Model from the CMIP5 model ensemble. This analysis is based on the simulation of snow cover dynamics on the surface and vertical heat transfer and unsaturated water flow in the topsoil and the underlying unsaturated zone. The thermophysical and hydrophysical input parameters were obtained from the inversing of the temperature data at observation sites on the territory of the Moscow State University Zvenigorod Biological Station. The epignosic simulations of freezing depth during the period of 1945–2015 have shown a decreasing trend for a period starting from 1940s through the early 1990s, with its subsequent stabilization in the late 20th and early 21st century. Predictions of seasonal freezing depth for the second half of the 21st century involved generation of three stationary meteorological time series of diurnal resolution (each spanning 100 years for the periods of 2020–2040, 2040–2060 and 2060–2080) for all of the circulation models utilizing the RCP8.5 greenhouse gas emission scenario. These series were used as boundary conditions in modeling of intra-annual dynamics of the snow cover depth at earth's surface, and heat and moisture transfer dynamics in the underlying subsurface zone. The simulation results analysis revealed reduction of the thickness of the seasonally frozen layer and reduction by at least a month (by the 2060s and 2080s of the 21st century) of soil freezing duration due to earlier onset of steady air temperatures above zero degrees Celsius in the spring. Given those results of the heat transfer and water flow simulations for five different climate projections still differ significantly one from other, they do not allow to provide any reliable predictions of the long-term dynamics of seasonal freezing depth in the second half of the 21st century.

*Depth of freezing, modeling, heat transfer and water flow, unsaturated zone, seasonally frozen layer, climate change, the thermal regime of soil*

## INTRODUCTION

Effects of current (observed) and predicted climate changes on the surface heat balance and heat transfer between soil surface and the atmosphere have been intensively studied over the last decades. Most often, analysis of changes in the thermal regime of soils is focused on the areas of permafrost distribution, due to the increasingly arising problems of its degradation and affiliated increase in the layer of seasonal thaw (i.e. active layer, AL). Examples of such studies can be found in [*Anisimov, 2009; Pavlov et al., 2010; Arzhanov et al., 2013; Koven et al., 2013*].

The problem of observed and predicted variability of seasonal freeze depth (SFD) is studied less extensively, though. The temperature dynamics analysis based on the data from a number of Russian weather stations (WS) over the last 40 years [*Sherstyukov, 2008*] indicates that long-term temperature changes within the 80–320 cm depth interval in the European Russia beyond the limits of the permafrost zone correlate well with air temperature variations, producing a warming trend in the shallow subsurface.

Analysis of field data and modelling coupled heat transfer and vertical water flow in the freezing/thawing soils [*Kalyuzhny and Lavrov, 2016*] has shown reducing trends (since the mid-1980s) for seasonal soil freezing depth in the Volga river basin.

The forecast of variations in the thermal regime of soils in the 21st century shows a good correlation with the predicted variability of air temperatures and precipitation patterns derived from global and regional atmosphere–ocean general circulation models (AO-GSMs). The insights provided in [*Anisimov and Kokorev, 2017*] suggest that, given a significant uncertainty of results yielded by various AO-GCMs, any sufficiently reliable forecasting appears problematic

today; anyway, the range of this uncertainty is tending to decrease with advancements in climate modeling, thereby improving the accuracy.

Despite the existing AO-GCMs being often justifiably criticized, for example from the perspective of description of the solar radiation block [*Fedorov, 2019*], they allow the climatologists to generate climate change projections to mid and end of the 21st century, involving the scenario analysis approach, and to utilize them for analyses of the potential changes in water resources, crop yield, etc.

Note that from the standpoint of the thermal regime, this uncertainty involves both the predicted factors: air temperatures and amount of precipitation. The effect of temperatures is generally recognized as follows: the higher is the winter temperatures, the shallower is the depth of seasonal freezing. At this, the AO-GCMs results for the European part of Russia project the growth of mean annual temperatures in the 21st century, while its magnitude is largely dictated by the greenhouse gas emission scenario. Whereas the precipitation pattern is more complicated, inasmuch as the predicted variations change from model to model, and their effect on the seasonal thaw dynamics has proven not so obvious.

As is known, however, an increase in precipitation should lead to a decrease in SFD, due to a potential increase in soil moisture and thermal resistance of snow cover. An anticipated decrease in the average snow cover depth (SCD) driven by increased winter temperatures will be offset by additional precipitation in the AO-GCMs predicting prolific precipitation for the cold season. A decrease in precipitation, especially during the cold period, provides natural restrains to the SFD by reducing the soil moisture content and thermal resistance of the snow cover. However, effects of the coupling of temperature and precipitation on the predicted SFD dynamics can be analyzed only with use of dynamic models that jointly describe variations in SCD and heat and moisture transfer in soils.

The research aims to provide a quantitative analysis of the projected SFD dynamics in the 21st century utilizing the AO-GCMs-derived climate projections based on CMIP5, a new multi-model ensemble of models [*Semenov and Stratonovitch, 2015*] on the basis of SCD and the vertical heat fluxes in the underlying unsaturated zone dynamics modeling. The research methods have amounted to:

1. Justification and verification of the heat and moisture fluxes model parameters derived from soil temperature observations.

2. Epignostic modeling (solution of inverse problems) of SFD dynamics in the second half of the 20th and early in the 21st century based on actual temperature and precipitation measurements.

3. Generation of precipitation and temperature time series for five AO-GCMs selected within CMIP5.

4. Forecasting simulations of SFD dynamics using generated series and comparative analysis of the results for different AO-GCMs.

In contrast to most of the above mentioned works, this study considers the heat and moisture transfer simulation as one-dimensional, "landscape" model, inasmuch as the main objective is to reveal the differences in soil thermal regime responses to various AO-GCMs-generated climate projections.

## MATHEMATICAL MODEL OF THE ACTIVE LAYER THICKNESS DYNAMICS

The Surfbal model [*Grinevskyi and Pozdniakov, 2017; Pozdniakov et al., 2019*] was used in the SFD dynamics modeling to factor into the warming effect of the snow cover. The model consists of three interrelated calculation blocks (submodels): precipitation transformation on the surface during the year; potential evapotranspiration and heat transfer; and water flow in the unsaturated zone. The Surfbal model uses long-term daily precipitation and snow water equivalent (SWE) series, relative air moisture content, minimum and maximum air temperatures, wind speed, and surface incident solar radiation measured or recovered from the daily minimum and maximum temperatures as meteorological inputs.

The Surfbal precipitation transformation submodel allowing calculating snow accumulation, consolidation and melting includes the seasonal snow cover dynamics model developed by A.N. Gel'fan and Yu.G. Motovilov and found to be well-proven in these processes modeling at the catchment scale for the Central Russia [*Gel'fan and Moreido, 2014*]. This model estimates the dynamics of snow accumulation and loss at the point, taking into account the major controls of the snow cover depth and its density, which include: snow accumulation from precipitation, its loses during melting and transpiration, snow compaction due to an increase in the current average density compared to the density of freshly precipitated snow.

Horizontal, wind-induced snow transport is not taken into account in this model, while melt water consumption is split between surface runoff and infiltration. The Gel'fan–Motovilov model allows estimating the dynamics of snow water equivalent, snow depth and average snowpack density at the point, utilizing (in line with the Surfbal model) the same meteorological input data derived from daily measurements, such as: diurnal precipitation, maximum and minimum air temperatures.

A one-dimensional vertical heat transfer equation with account of phase transitions interpreted as continuous throughout the below zero temperature

range is used to estimate the soil temperature dynamics in the Surfbal program:

$$C_s \frac{\partial T}{\partial t} - L_i \rho_i \frac{\partial \theta_i}{\partial t} = \frac{\partial q_T}{\partial z},$$

$$q_T = -\lambda_{ef}\left(T, \theta_w, \theta_i\right)\frac{\partial T}{\partial z} + C_w T v_z, \qquad (1)$$

$$C_s = \left(1-\theta_{max}\right)C_r + \theta_w C_w + \theta_i C_i + \left(\theta_{max} - \theta_w - \theta_i\right)C_{air},$$

where $T$ is temperature; $\theta_i$ is volumetric ice content; $\theta_w$ is volumetric water content; $\theta_{max}$ is porosity; $L_i$ is latent heat of ice fusion; $C_s$ is additive volumetric heat capacity of soil, as a sum of products of the phases of volumetric heat capacities $C$ (with appropriate subscripts: *r* for the solid rock phase, *w* for water, *i* for ice, and *air* for air) by the volume fraction of each phase; $\lambda_{ef}$ is soil thermal conductivity coefficient , taking into account of the actual content of water $\theta_w$ and ice $\theta_i$ at given temperature $T$; $q_T$ is vertical heat flux; $t$ is time; $z$ is vertical coordinate; $v_z$ is the vertical water flow rate calculated by solving the unsaturated water flow equation in porous medium conjugated to (1).

Modeling water phase transitions continuous over the entire negative temperature range using equation (1) after [*Dall'Amico et al., 2011*] and the van Genuchten's equation of state generalized to negative temperatures in the submodel of heat transfer linking the mobile water content θ in soil with the suction head $h(\theta)$:

$$h(\theta) = -\alpha^{-1}\left(S^m - 1\right)^{1/n}, \quad S = \frac{\theta - \theta_{min}}{\theta_{max} - \theta_{min}}, \qquad (2)$$

where $\alpha$, $m$, $n$ are van Genuchten empirical parameters selected by minimizing the deviations calculated by function (2) of suction heads and their measured experimental values at known moisture content.

While at subzero temperatures, the suction head $h_T(\theta_w, T)$ is largely dictated by both the content of unfrozen water $\theta_w$ and temperature:

$$h_T\left(\theta_w, T\right) = \begin{cases} h(\theta), & T > T^*, \\ h(\theta) + a_T\left(T - T^*\right), & T \le T^*, \end{cases}$$
$$T^* = -a_T^{-1} h(\theta), \quad a_T = \frac{g T_0^a}{L_i}, \qquad (3)$$

where $T^*$ is the freezing point of water at a given moisture content; $T_0^a$ = 273.16 °C; $h(\theta)$ is the suction head calculated using the van Genuchten equation (2); the subscript $T$ in the formula for suction head $h_T(\theta_w, T)$ of unfrozen water in the low-temperature environment shows that this head depends on temperature. An expression for the average pore saturation with mobile water in the presence of ice $S$ is defined as

$$S\left[h_T\left(\theta_w, T\right)\right] = \frac{\theta_w - \theta_{min}}{\theta_{max} - \left(\theta_i + \theta_{min}\right)}, \qquad (4)$$

where $\theta_{max}$ is the maximum volumetric moisture content; $\theta_{min}$ is the residual water content which that is not moved by gravity and suction head gradients.

The volume content of ice $\theta_i$ at a given negative temperature is thus determined as the difference between the total moisture content at a positive temperature and the content of unfrozen water at a subzero temperature:

$$\theta_i = \left(S(h) - S\left(h_T\right)\right)\frac{\theta_{max} - \theta_{min}}{\theta_{max} - \theta_{min} + \left(S(h) - S\left(h_T\right)\right)}. \qquad (5)$$

The use of equations (1)–(5) with no water flow conditions included allows estimating the thermal regime for a case when total moisture content remains constant at each point of the calculated profile, with only phase-changes taking place, i.e. $d\theta_i = -\frac{\rho_w}{\rho_i} d\theta_w$.

If equation (1) is coupled with the unsaturated flow equation, then, while solving them simultaneously, the time-variable total moisture content $\theta = \theta_w + \theta_i$ is analyzed at each calculated point of the profile.

In equation (1), the coefficient of thermal conductivity of soils $\lambda_{ef}$ depends on the matrix thermal conductivity, as well as water contents and phase composition. The Coté and Konrad algorithm [*Côté and Konrad, 2005*] is included into the Surfbal code for this dependence parameterization and calculation of thermal conductivity coefficient for a specified pore saturation with mobile water.

The nonlinear interpolation between the values of thermal conductivity in fully water-saturated ($\lambda_{sat}$) (at known volume ice content) and dry ($\lambda_{dry}$) states over the entire range of positive and negative temperatures takes the form of:

$$\overline{\lambda}(S) = \frac{\lambda(S) - \lambda_{dry}}{\lambda_{sat} - \lambda_{dry}} = \frac{\kappa S}{1 + (\kappa - 1)S},$$

where $\kappa$ is an empirical parameter controlled by rocks lithology and their state (frozen, unfrozen).

Modeling the temperature waves propagation from the surface to the unsaturated zone requires the knowledge of the temperature of the underlying surface, which is: vegetation cover (in the summer) and snow surface (in the winter). At this, the Surfbal software uses the available surface air temperature (SAT) data at the meteorological measurement height, as input data.

The general boundary condition [*Pozdnyakov et al., 2019*] was used in the current version of Surfbal specifies the transition from air temperature ($T_{air}$) to the underlying surface temperature ($T_{soil}$) and is written as

$$\frac{T_{\text{air}} + \Delta T(t) - T_{\text{soil}}(0)}{R_{\text{air}} + R_{\text{surf}}} = -\lambda_{\text{ef}}\left(T_{\text{soil}}\right)\frac{\partial T_{\text{soil}}}{\partial z}\bigg|_{z=0}, \quad (6)$$

where $\Delta T(t)$ is the difference between temperatures of air and the underlying surface caused by the radiation heating (summer season) and cooling (winter season), as a given function with annual periodicity. Its parameterization is discussed in greater detail in [*Pozdnyakov et al., 2019*].

The denominator in the left part of the boundary condition (6) is the sum of thermal resistances of the underlying surface ($R_{\text{surf}}$) and the air ($R_{\text{air}}$), both being responsible for the intensity of heat transfer between the underlying surface and the meteorological measurement height. Parametrization of these resistances in the Surfbal software is shown below. As an overwinter parameter, $R_{\text{surf}}$ is defined as

$$R_{\text{surf}} = \int_0^H \lambda_{\text{sn}}^{-1}(z)dz + R_0,$$

where $H$ is the present snow cover depth with a thermal conductivity coefficient $\lambda_{\text{sn}}$. In the warm season, characterized as snow-free, $R_{\text{surf}}$ is the thermal resistance of forest/field leaf-floor $R_0$, when available.

The air resistance $R_{\text{air}}$ is determined as

$$R_{\text{air}} = \left(\frac{C_{\text{air}}}{r_a} + 4\sigma\varepsilon_s\left(T_{\text{air}} + T_0^a\right)^3\right)^{-1},$$

where $\sigma$ is the Stefan–Boltzmann constant; $\varepsilon_s$ is the emission factor of the underlying surface, while for the surfaces of snow/moistened soil, the parameter $\varepsilon_s$ value can be assumed to be equal to one; $r_a$ is the air resistance [s/m] controlled by the wind speed and two reference heights (vegetation height and meteorological measurement height [*Allen et al., 1998*]) and calculated in the Surfbal evapotranspiration submodel.

Equation (6) is used as a boundary condition on the surface in the warm and cold seasons, with no snowmelt. During the snowmelt, the temperature on the underlying surface, i.e. the snow surface, is assumed to be known and equal to zero, inasmuch as all the heat entering this surface is consumed by the snowmelt.

Therefore, for this particular period, equation (5) is used as a boundary condition at $T_{\text{air}} + \Delta T = 0$ and $R_{\text{air}} = 0$.

## EPIGNOSTIC AND RETROSPECTIVE MODELING

The thermal regime modeling was based on the results obtained from the unsaturated zone heat-and-moisture transfer monitoring sites on the territory of the Zvenigorod Biological Station of Moscow State University [*Grinevskyi et al., 2011*]. The two additional monitoring sites were designed (and accordingly located) as distinctly representative of the field and forest environments. The unsaturated zone temperature monitoring have been run since 2009 within them, with the automatic temperature data loggers installed at depths of 0.25, 0.5, 0.8 and 1.5 m from the surface. The surface layer of sites constitutes natural vegetation on the first above-floodplain terrace of the Moskva river. In terms of lithology, sediments composing the unsaturated zone are loamy (field site) and sandy loamy (forest site).

Key characteristics of soils were derived from laboratory analyses of the samples with undisturbed structure (hydrophysical characteristics) and from the experimental determinations in the test pit using MIT-1, a thermal conductivity gauge (thermophysical characteristics)

Using the model described above, the heat-and-moisture transfer in the unsaturated zone was simulated for these sites with the focus on the epignosic period (2009–2016). Figure 1 shows the epigenosic modeling results compared to the observational data, which is discussed in greater detail in [*Pozdnyakov et al., 2019*].

In the heat transfer simulations, the daily snow depth and snowpack density data derived from the precipitation transformation submodel were translated into the snow thermal resistance using Sturm's function of thermal conductivity $\lambda_{\text{sn}}$ to snow density $\rho_{\text{sn}}$ [*Sturm et al., 1997*]:

$$\lambda_{\text{sn}} = \begin{cases} 2.3\cdot10^{-2} + 2.34\cdot10^{-4}\rho_{\text{sn}},\ \rho_{\text{sn}} \le 156\ \text{kg/m}^3, \\ 0.138 - 1.01\cdot10^{-3}\rho_{\text{sn}} + 3.233\cdot10^{-6}\rho_{\text{sn}}^2,\ \rho_{\text{sn}} > 156\ \text{kg/m}^3. \end{cases}$$

A retrospective simulation of heat transfer in the second half of the 20th–early 21st centuries based on the field site section and observational data on the air temperatures and precipitation dynamics was selected for further research.

Given that the meteorological observations data from the Zvenigorod test site are restrained by relatively short series, the observational time series from the nearest Mozhaisk weather station were used as input meteorological data. These were preferred due to their high correlation (in regard to maximum and minimum daily air temperatures and monthly precipitation) with the Zvenigorod WS data.

Daily meteorological time series for 1945–2015 selected as a boundary condition on the surface were based on the Mozhaysk station data, while water- and thermophysical characteristics of the section were inferred from the experimental and model calibration data for the Zvenigorod field site. Results of the calculation of the annual maximum penetration depth of the zero isotherm, i.e. the maximum depth of frost front penetration are shown in Fig. 2. The study [*Pozdnyakov et al., 2019*] showed that the zero isotherm penetration depth and its calculated overwinter dy-

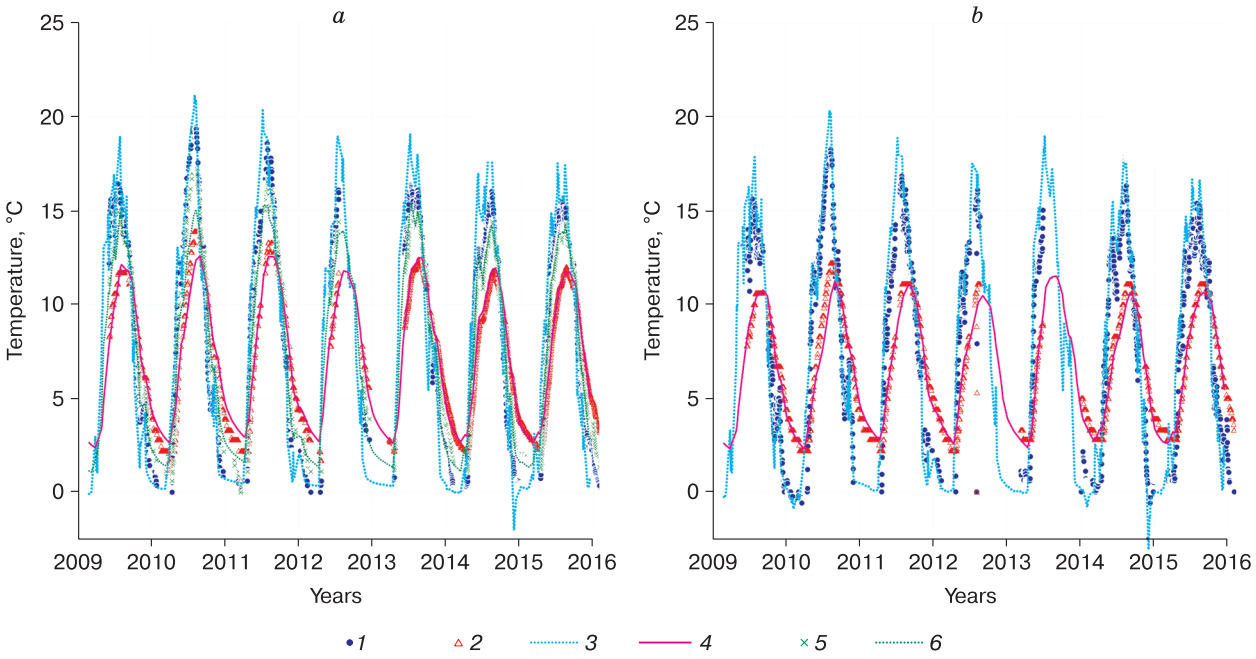


**Fig. 1. Comparison of the observed and model temperatures at the field (*a*) and forest (*b*) sites.**

*1* – measurements at a depth 0.25 m; *2* – measurements at a depth 1.5 m; *3* – model temperature at a depth 0.25 m; *4* – model temperature at a depth 1.5 m; *5* – measurements at a depth 0.8 m; *6* – model temperature at a depth 0.8 m.

namics in the investigated region are very sensitive to the choice of the model of a relationship between the snow thermal conductivity and its density. The calculations shown in Fig. 2 were therefore performed for two models of such relation based on: (1) the above mentioned Strum's function, and (2) the dependence according to *N.I. Osokin et al.* [*2013*], obtained by generalizing the best known empirical links between snow thermal conductivity and density:

$$\lambda_{sn} = 9.165 \cdot 10^{-2} - 3.814 \cdot 10^{-4} \rho_{sn} + 2.905 \cdot 10^{-6} \rho_{sn}^2 .$$

Regardless of the difference in the values, using the dependence after N.I. Osokin with other parameters unchanged yields the maximum penetration (15–20 cm deeper) of the zero isotherm (Fig. 2). The overview of the freezing depth curves smoothed by the local polynomials reveals that they all show a consistently decreasing trend from 40s to the mid-80s–early 90s, followed by some stabilization in the late 20th and early 21st centuries.

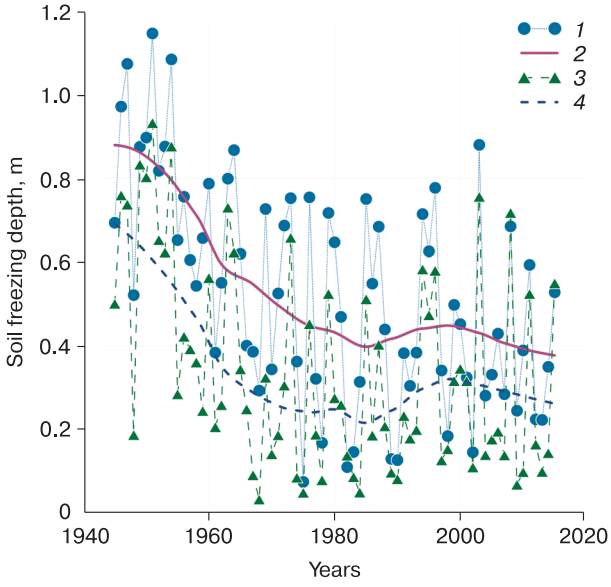


**Fig. 2. Results of retrospective modeling of soil freezing depth dynamics for the field site.**

*1* – model maximum soil freezing depth calculated as a function of snow thermal conductivity and snow density according to N.I. Osokin; *3* – model maximum soil freezing depth calculated as a function of snow thermal conductivity and snow density according to Strum et al.; *2*, *4* – local polynomial smoothing of the results, accordingly.

## SEASONAL FREEZE DEPTH VARIABILITY FORECASTING FOR THE 21st CENTURY

Forecasting seasonal freeze for the second half of the 21st century involved LARSWG 6.0, a stochastic weather generator [*Semenov and Stratonovitch, 2010, 2015*], whose sixth version allows forecasting daily time series for GCM of surface weather conditions in the CMIP5 multi-model ensemble [*Semenov and Stratonovitch, 2015*]. The meteorological time series Mozhaysk weather station was selected for generator setting over the period spanning 1945–2015, which

Table 1. **Characteristics of the predicted precipitation and temperature using different GCMs under the extreme greenhouse gas (GHG) emissions scenario (RCP8.5) over 2060–2080**

| No. | Model | Country | The 2060–2080 forecast for Moscow region | |
|---|---|---|---|---|
| | | | Total annual precipitation, mm | Mean annual air temperature (MAAT), °C |
| 1 | EC-EARTH | European Union | 761 | 8.15 |
| 2 | GFDL-CM3 | USA | 788 | 11.0 |
| 3 | HadGEM2-ES | Great Britain | 569 | 10.6 |
| 4 | MIROC5 | Japan | 673 | 10.2 |
| 5 | MPI-ESM-MR | Germany | 678 | 7.8 |
| 6 | Basic time series (1945–2015) | | 626 | 4.7 |

served as a basis for retrospective calculation of soil freezing depth. The LARSWG 6.0 includes five models, whose characteristics are listed in the Table 1.

Three stationary meteorological time series of diurnal resolution, each spanning one hundred years for the periods of 2020–2040, 2040–2060 and 2060–2080, were generated for all of the circulation models in Table 1 utilizing the RCP8.5 greenhouse gas emission scenario. The choice of a centurial modeling period for each of the 20-year meteorological time series is explained by the necessity of obtaining steady time-averaged characteristics of seasonal thaw, including: the average long-term expected intra-annual SFD dynamics and the average long-term maximum freezing depth for each of the selected intervals. That

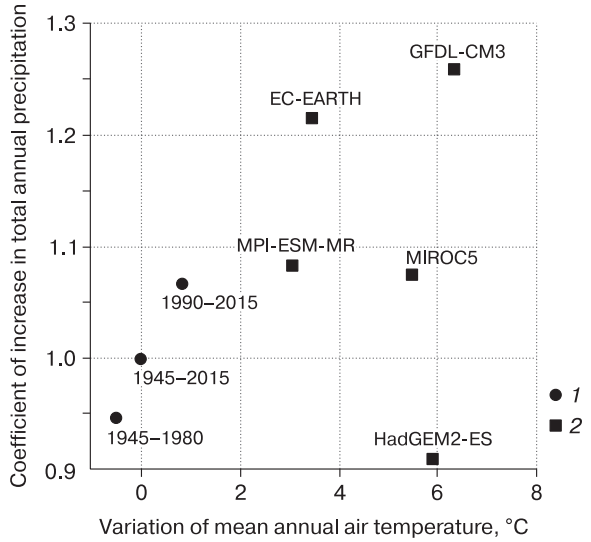


**Fig. 3. Variations of mean annual air temperature and total annual precipitation versus the basic time series.**

*1* – observational data; *2* – generated time series for the period of 2060–2080 under extreme greenhouse gas emission scenario (RCP8.5). At the top above the symbol is shown the name for the time series forecasting model, at the bottom is the averaging period for observed time series.

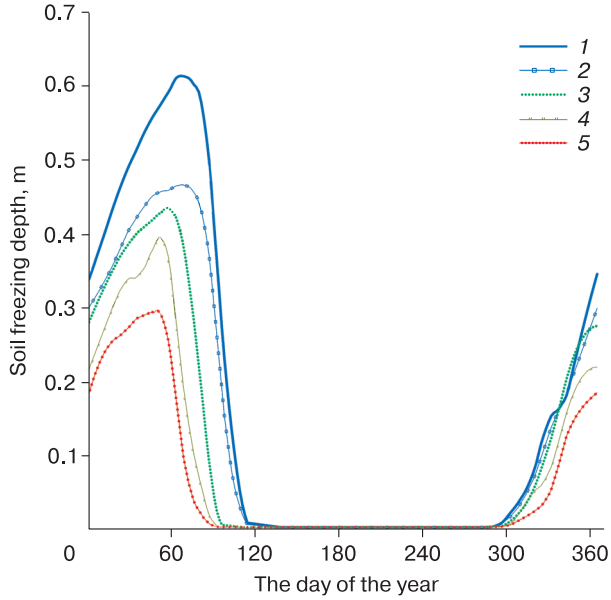


**Fig. 4. Mean multiyear intraannual dynamics of model soil freezing depth.**

Time intervals for averaging modeling results using actual time series (*1*, *2*) or forecasting time series for the EC-EARTH model (*3*–*5*).

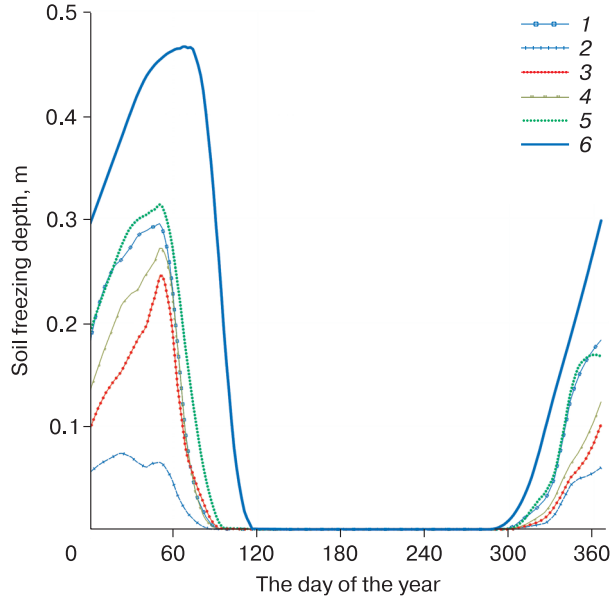


**Fig. 5. Comparison of mean multiyear maximum seasonal freezing depth for basic and forecasting time series for 2060–2080.**

*1*–*6* – models' numbers correspond to those listed in Table 1.

was exactly why statistically stationary time model series for each predicted interval significantly exceeded its length.

The generalized characteristics of the increase in average annual temperatures and the coefficient of variation of annual total precipitation in relation to the time series of initial observations for the Mozhaysk station for 1945–2015 are given in Fig. 3. Given that the initial meteorological data are characterized by long-term variability, Fig. 3 shows additional characteristics of temperature and precipitation variations for both the entire period (1945–2015), and for its starting (1945–1980) and terminal (1990–2015) parts.

Figure 3 demonstrates that all models predict an increase in mean annual temperatures averaging from 3 to 6.5 °C, whereas only the HadGEM2-ES model forecasts a warmer and drier climate for the studied region. Interestingly, the temperature and precipitation dynamics plot (Fig. 3) shows that the results obtained from the EC-EARTH and GFDL-CM3 models appear to inherit the observed trend of climate change in the coordinates given in Fig. 3. The transformation of precipitation on the earth's surface and the distribution of soil temperatures in the unsaturated zone were modeled for each of the generated meteorological time series. Then the average long-term curve of the zero isotherm penetration depth characterizing the freezing depth is calculated by averaging each temperature series model.

N.I. Osokin's dependence was used in the forecasting simulations to link the density and snow thermal conductivity. The results of the calculated dynamics of the freezing depth averaged for the entire basic time series (1945–2015) and for the starting time-period (1945–1980) were compared with the forecasting results based on the time series generated by LARSWG utilizing the EC-EARTH model (Fig. 4).

Figure 4 clearly reflects the general pattern seen as the predicted decrease in the maximum average annual freezing depth and the earlier onset of the warm period in the spring, as compared to the 20$^{th}$ century. Almost the same comparison, but for the period of 2060–2080, is shown in Fig. 5, performed for the five generated time series, according to the forecasting climate models in Table 1. Despite the fact that all tested models yield a significant decrease in the maximum average long-term freezing depth, the differences between the models are large enough to give a confidently predict the magnitude of such decrease (Fig. 5).

Based on the results of simulating for the period 2060–2080, the maximum values of freezing depth, snow water equivalent (SWE) of the snow cover and snow depth were determined for each model year to characterize the annual spikes in freezing depth, SWE in the snowpack, and snow depth. The average values and standard deviations of these characteristics are listed in Table 2 and compared with the same characteristics resulted from the epignostic modeling. Thus, Fig. 5 describes the expected average long-term curve of the freezing depths distribution within the year, while the average rates of the annual maximum values of freezing depths, SWE and snow depth are given in Table 2.

It follows from Table 2 that the maximum annual freezing depth will be decreased by 10 cm or less compared to observation series despite the increase in temperatures obtained for four of the five tested models. This is associated with a more than two-fold decrease in the maximum snow depth, i.e. its warming effect is decreasing.

The GFDL-CM3 model has shown almost twice as little value of the maximum freezing depth, while the maximum SWE and depth of snow differ little from other models; the total precipitation is found to be the largest. In this model, a decline in the maximum freezing depth appears to be affected by the general increase (including overwinter) in water absorption, entailing an increase in soil moisture content and, accordingly, to an increase in heat loss because of phase changes.

Table 2. **Statistical characteristics of maximum soil freezing depths and snow water equivalent (SWE), snow cover depth in forecasts for 2060–2080 using different GCMs under the extreme greenhouse gas (GHG) emissions scenario (RCP8.5)**

| Statistical characteristics | Model | | | | | Basic time series (1945–2015) |
|---|---|---|---|---|---|---|
| | EC-EARTH | GFDL-CM3 | HadGEM2-ES | MIROC5 | MPI-ESM-MR | |
| Mean multiyear maximum soil freezing depth, m | 0.48 | 0.28 | 0.42 | 0.46 | 0.50 | 0.53 |
| Standard deviation in freezing depth, m | 0.14 | 0.08 | 0.10 | 0.10 | 0.12 | 0.26 |
| Mean multiyear maximum snow water equivalent (SWE), mm | 35.1 | 20.5 | 20.2 | 21.6 | 31.6 | 94.2 |
| Standard deviation in SWE, mm | 16.7 | 9.1 | 10.2 | 8.9 | 15.7 | 44.9 |
| Mean multiyear maximum snow cover depth (SCD), cm | 20.7 | 13.7 | 13.3 | 14.0 | 19.0 | 38.7 |
| Standard deviation in SCD, cm | 7.1 | 5.6 | 5.9 | 5.0 | 7.1 | 14.9 |

The average long-term freezing depths derived from the forecast modeling results (for three time intervals and five predictive models) and complemented by epignostic calculations are presented in Fig. 6. Note that the results for each calculation period are assigned to the midpoint on the time scale, while symbols magnitude in this figure is scaled according to the maximum snow cover depth. The maximum symbol magnitude corresponds to the snow depth of 30 cm and decreases linearly until it becomes equal to zero. The point corresponding to the period of 2040–2060 is unavailable for the GFDL-CM3 model due to the impossibility to generate meteorological time series covering this period in the LARS WG 6.0 version of this model. The results shown in Fig. 6 revealed a significant difference in the average long-term freezing depth obtained by different models for each period. These show however an obvious trend: the less the model predicts the temperature excess over the basic time series (Table 1), the greater the predicted average annual freezing depth obtained therefrom.

Result of the GFDL (Geophysical Fluid Dynamics Laboratory of Princeton University) Climate Model version 3 (CM3) predicting warm season precipitation anomalies (extreme warm and wet) was quite unexpected. Despite the extreme nature of the predicted climate change, specifically this model was found to "inherit" the retrospective modeling results (Fig. 6). However, answering the question as to whether this result is explicable or incidental requires additional analyses of the data from other weather stations in the region.

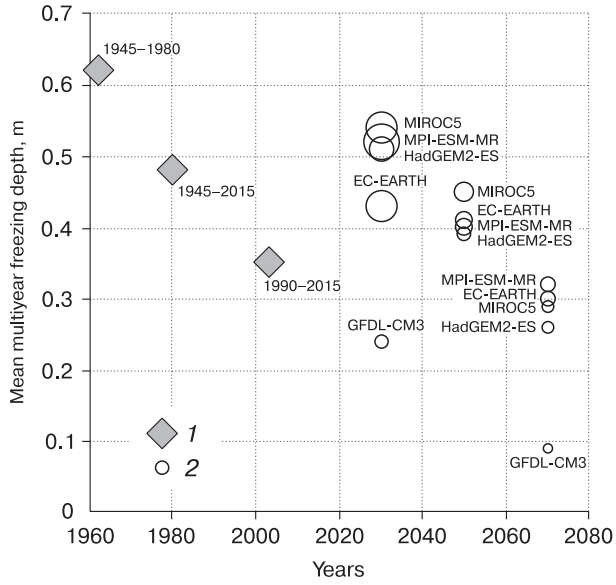


**Fig. 6. Mean multiyear maximum soil freezing depth for epignostic (*1*) and forecasting (*2*) modeling.**

Next to the symbol are shown either time intervals for averaging retrospective modeling results or the name of forecasting model.

## CONCLUSIONS

The studies allow an inference about perspectivity of the considered approach for using the results obtained by global and regional GCMs in the analysis of precipitation transformation on the surface and heat transfer and water flow in the unsaturated zone described by the local (landscape) dynamics models. Specifically this approach allowed us to reveal how the observed and forecast trends in climate change grade into changes in thermal fields in the shallow subsurface and become manifested in the snow cover depth and seasonal freeze depth dynamics, as well as to assess the uncertainties in forecasting such transformations.

The simulation studies on the example of a type section of rocks of the unsaturated zone and Moscow region-specific conditions confirm the generally reducing trend in the average seasonal freezing depth generated by the results of observations in the late 20$^{th}$ and early 21$^{st}$ centuries [*Kalyuzhny and Lavrov, 2016*].

The efforts made to predict active layer thickness dynamics over the 21$^{st}$ century based on the climate variability predicted by last generation AO-GCMs have shown in varying degrees that all the used models produce a decreasing trends to the 60–80s of the 21$^{st}$ century for SFD and for the time-period during which the soil freezing takes place in the unsaturated zone, due to one month or even more earlier onset of steady air temperatures above zero degrees Celsius in spring.

However, the differences between the modeling results obtained on the base of the precipitation and temperature series generation for different forecast GCMs are still significant, precluding thereby reliable long-term forecasts for freezing depth dynamics for the second half of the 21$^{st}$ century.

*The work was finically supported by the Russian Science Foundation, RSF (grant No. 16-17-10187).*

## References

Allen, R.G., Pereira, S., Raes, D., Smith, M., 1998. Crop evapotranspiration guidelines for computing crop water requirements. FAO Irrigation and Drainage. Paper 56, Food and Agriculture Organization of the United Nations, 15 pp.

Anisimov, O.A., 2009. Stochastic modelling of the active layer thickness under conditions of the current and future climate. Kriosfera Zemli (Earth's Cryosphere), XIII (3), 36–44.

Anisimov, O.A., Kokorev, V.A., 2017. Russian permafrost in the 21$^{st}$ century: model-based projections and analysis of uncertainties. Earth's Cryosphere XXI (2), 3–9.

Arzhanov, M.M., Yeliseyev, A.V., Mokhov, I.I., 2013. The influence of climatic changes over the land of extratropical lati-

tudes on the dynamics of permafrost soils under RCP scenarios in the 21st century according to the calculations of the global climate model of the IAP RAS. Meteorologia i Gidrologia (Meteorology and Hydrology), No. 7, 31–42.

Côté, J., Konrad, J.-M., 2005. A generalized thermal conductivity model for soils and construction materials. Can. Geotechn. J. 42 (2), 443–458, https://doi.org/10.1139/t04-106.

Dall'Amico, M., Endrizzi, S., Gruber, S., Rigon, R., 2011. A robust and energy-conserving model of freezing variably-saturated soil. The Cryosphere, vol. 5, 469–484, http://doi.org/10.5194/tc-5-469-2011.

Fedorov, V.M., 2019. Variations of the earth's insolation and especially their integration in physical and mathematical models of the climate. Uspekhi Fizicheskikh Nauk 62 (1), 32–45.

Gel'fan, A.N., Moreido, V.M., 2014. Dynamic stochastic modeling of snow cover formation in the European territory of Russia. Led i Sneg (Ice and Snow), 136 (2), 44–52.

Grinevskyi, S.O., Maslov, A.A., Pozdniakov, S.P., 2011. The experience in the creation and application of a complex of regime hydrogeological observations in the conditions of the Zvenigorod test site of the Lomonosov Moscow State University. Inzhenernye Izyskania (Engineering Survey), No. 5, 30–34.

Grinevskyi, S.O., Pozdniakov, S.P., 2017. A retrospective analysis of the impact of climate change on the formation of groundwater resources. Moscow University Geology Bulletin 72 (3), 200–208.

Kalyuzhny, I.L., Lavrov, S.A., 2016. The influence of climate changes on soil freezing depth in the Volga river basin. Led i Sneg (Ice and Snow), 56 (2), 207–220.

Koven, C.D., Riley, W.J., Stern, A., 2013. Analysis of permafrost thermal dynamics and response to climate change in the CMIP5 Earth System Models. J. Climate, No. 26, 1877–1900.

Osokin, N.I., Sosnovskiy, A.V., Chernov, R.A., 2013. The influence of the stratigraphy of the snow cover on its thermal resistance. Led i Sneg (Ice and Snow), 53 (3), 63–70.

Pavlov, A.V., Perlstein, G.Z., Tipenko, G.S., 2010. Actual aspects of modeling and prediction of the permafrost thermal state under climate change conditions. Kriosfera Zemli (Earth's Cryosphere), XIV (1), 3–12.

Pozdnyakov, S.P., Grinevskyi, S.O., Dediulina, E.A., Koreko, E.S., 2019. The sensitivity of seasonal freezing simulation to the computational model of the thermal conductivity of snow cover. Led i Sneg (Ice and Snow), 59 (1), 67–80.

Semenov, M.A., Stratonovitch, P., 2010. The use of multi-model ensembles from global climate models for impact assessments of climate change. Climate Res. 41, 1–14.

Semenov, M.A., Stratonovitch, P., 2015. Adapting wheat ideotypes for climate change: accounting for uncertainties in CMIP5 climate projections. Climate Res. 65, 123–139, DOI: 10.3354/cr01297.

Sherstyukov, A.V., 2008. Correlation of soil temperature with air temperature and snow cover depth in Russia. Kriosfera Zemli (Earth's Cryosphere), XII (1), 79–87.

Sturm, M., Holmgren, J., Konig, M., Morris, K., 1997. The thermal conductivity of seasonal snow. J. Glaciol. 43 (143), 26–41.

*Received September 28, 2018*
*Revised version received February 21, 2019*
*Accepted April 18, 2019*